DISCLAIMER

This report was prepared as an account of work sponsored by an agency of the United States Government. Neither the United States Government nor any agency thereof, nor any of their employees, makes any warranty, express or implied, or assumes any legal liability or responsibility for the accuracy, completeness, or usefulness of any information, apparatus, product, or process disclosed, or represents that its use would not infringe privately owned rights. Reference herein to any specific commercial product, process, or service by trade name, trademark, manufacturer, or otherwise does not necessarily constitute or imply its endorsement, recommendation, or favoring by the United States Government or any agency thereof. The views and opinions of authors expressed herein do not necessarily state or reflect those of the United States Government or any agency thereof. Reference herein to any social initiative (including but not limited to Diversity, Equity, and Inclusion (DEI); Community Benefits Plans (CBP); Justice 40; etc.) is made by the Author independent of any current requirement by the United States Government and does not constitute or imply endorsement, recommendation, or support by the United States Government or any agency thereof.

Effects of Internal and External Heat Sources on Cladding Microstructure and Rupture Performance

Nuclear Technology Research and Development

Prepared for
U.S. Department of Energy

Mackenzie Ridley
Brandon Johnston
Samuel Bell
Nathan Capps
Oak Ridge National Laboratory
05/30/2025
M3FT-25OR020202043
ORNL/SPR-2025/3923

SUMMARY

In the event of a Loss of Coolant Accident (LOCA), the primary supply of cooling water for a nuclear reactor is lost, leading to a significant pressure differential across the cladding wall. Without adequate cooling, the fuel rods continue to heat as a result of fission reactions. Research at Oak Ridge National Laboratory's (ORNL's) Severe Accident Test Station (SATS) is currently focused on evaluating fuel cladding performance using an external infrared lamp as a heat source, whereas legacy testing primarily utilized an internal heating approach. While external heating may better simulate the effect of neighboring fuel rods heating a central rod, it may not accurately represent the internal heat absorption from the fuel during accident transients. The heating dynamics depend greatly on the fuel rod's position within the bundle and the reactor. To fully understand the implications of a LOCA event and assess the influence of internal heating on cladding performance, combined internal heating and pressurization capability was developed at ORNL. Tests were conducted to compare cladding segments heated internally (representing heat from the fuel within the rod) and externally (representing heat from adjacent fuel rods). The findings indicate that both internal and external heating result in comparable rupture temperatures during 5°C/s laboratory LOCA tests and also agree with legacy test data. Axial temperature gradients and internal heat source dispersal were found to significantly impact cladding deformation and rupture geometry. Clear modifications were outlined to further improve the capability with heating rates above 5°C/s.

CONTENTS

FIGURES

TABLES

ACRONYMS

ATF	Accident-tolerant Fuel
DOE	Department of Energy
EBSD	Electron Backscatter Diffraction
ECCS	Emergency Core Cooling System
ID	Inner Diameter
IR	Infra-red
LOCA	Loss-of-coolant Accident
LWR	Light Water Reactor
NRC	Nuclear Regulatory Commission
MRBT	Multi-rod Burst Test Program
OD	Outer Diameter
ORNL	Oak Ridge National Laboratory
PWR	Pressurized Water Reactor
SATS	Severe Accident Test Station
Zry-4	Zircaloy-4

LOSS OF COOLANT ACCIDENT TESTING

1. INTRODUCTION

Understanding and establishing safety limits for postulated nuclear accidents has been a priority for research and development since the inception of early nuclear reactors. One of the most evaluated accident scenarios for light water reactors (LWRs) is a loss-of-coolant accident (LOCA), which occurs when there is a breach in the coolant system. The lack of coolant supply leads to the rapid flashing of residual water into steam, creating a situation with insufficient removal of decay heat that can rapidly drive temperatures upward. Alongside the rise in temperature, the drop in coolant pressure generates a positive pressure differential along the cladding walls due to the accumulation of gaseous fission products during operation. The combination of rapidly increasing temperatures and the resulting hoop stress on the cladding can lead to cladding rupture, which poses risks for a loss of long-term coolable cladding geometry, and potential release of radiation source terms through fuel fragmentation, relocation, and dispersal. Additionally, Zirconium alloys, the standard fuel cladding material class [1], generate zirconium dioxide (ZrO_2) and hydrogen (H_2) as a gaseous byproduct in high-temperature steam environments [2], raising concerns about combustion risks.

In reactor safety, accidents fall into one of two categories: (1) design basis, defined as the set of accidents that a reactor is designed to withstand without significant damage to the core or the release of radioactive materials and (2) beyond-design basis, which encompasses more severe events that exceed the assumptions and capabilities of the original design. These may include scenarios that are less likely to occur or have a very low probability, but still pose significant risks, such as large seismic events, large-scale floods, or catastrophic failures of safety systems, such as the events at the Fukushima disaster. Under design-basis LOCAs, it is assumed that the emergency core cooling system (ECCS) will respond adequately to flood the reactor core and re-establish cooling capacity in accordance with U.S. regulations 10 CFR § 50.46 based on zirconium where peak cladding temperature does not exceed 1204 °C and less than 17% of an equivalent cladding has reacted with high temperature steam.

Significant research efforts has been conducted at ORNL over the past 50 years to better define safety and operational margins for LWRs. Legacy fuel cladding accident testing was spearheaded by Nuclear Regulatory Commission (NRC) support through programs such as the Multirod Burst Test Program (MRBT) in the 1970’s and early 1980’s. In general, LOCA burst testing utilizes an internally pressurized cladding segment and a heat source to generate cladding failure via transient temperatures. Capabilities were established for both single rod and rod bundle testing, across a range of international institutions with variations in experimental setups.

Experimental results were often dictated by the methodology chosen to perform the burst testing, with dependence on a wide range factors from the test train assembly to the heating environment. For example, Chung and Kassner showed that utilizing stacked filler rod segments, to simulate stacked fuel pellets in a cladding, resulted in less defined balloon geometries than if a single length filler rod was used for laboratory LOCA testing [3]. The test gas environment (i.e. steam, air, or argon flow around the cladding outer diameter) has been shown to impact balloon geometry during LOCA testing [4]. Heating rate dependencies were defined along with a stress-based failure criteria for Zr alloy cladding [5]. While postulated LOCA’s could experience heating rates well above 100°C/s, it has been determined that there are minimal effects of heating rate on the cladding rupture temperature above 28°C/s [5]. Therefore, the majority of laboratory testing has been conducted with 0 – 28°C/s heating rates, although select testing such as the

inpile 7-rod bundle TREAT tests (up to 44°C/s) showcased heating rates above the defined threshold [6,7].

Legacy LOCA testing often utilized an internal heat source to simulate the decay heat source from fuel. Today, internal heating LOCA testing exist [8,9] but are not as common due to experimental complexities with environmental effects (i.e. oxidizing internal filaments upon rupture) and combined internal heating and internal pressurization. Having a heat source closer to cladding segment can enable higher heating rate testing capability and has the possibility to better control axial and azimuthal temperature gradients by reducing effects of experimental variations due to alignment such as in reflective infrared (IR) heating furnaces. Additionally, using an internal heat source could allow for improved equipment design to enhance quality of assessing cladding deformation *in situ*, such as with digital image correlation [10] or IR thermography. Therefore, a current task within the Department of Energy's (DOE) Advanced Fuels Campaign (AFC) is to revisit internal heating capability and assess performance trends relative to modern LOCA testing capabilities.

1.1 Legacy Internal Heating LOCA Testing at ORNL

At ORNL, the legacy MRBT internal heating tests generally employed a fuel pin simulator placed within a cladding segment. The use of these internal heaters significantly improved heating efficiency and allowed reliable tracking of local hot spots to predict potential rod failures and ensured comparability with expected performance of fueled cladding during temperature transients.

The fuel simulator consisted of a spiraled Kanthal heating element with a molybdenum oxide (MoO) core, surrounded by insulating boron nitride and housed within a stainless-steel sheath [11]. The entire assembly was reusable for multiple cladding transient tests. The outer diameter of the sheath was often coated with a plasma-sprayed zirconium oxide (ZrO_2) layer to prevent chemical interactions with the cladding. Axial grooves were machined into the sheath at 90-degree intervals, in which either sheathed thermocouples or thick gauge wires (made from tantalum, stainless steel, or nickel alloys) were placed. These wire placements served to center the fuel pin simulator within the cladding while maintaining a controlled gas gap between the inner diameter of the cladding and the outer diameter of the simulator. Fuel pin simulators were not placed throughout the entirety of the cladding segment. Instead, an upper region of the cladding was filled with ceramic inserts to provide a temperature gradient towards the sealed end of the cladding. This was likely introduced to ensure gas tightness with lower temperature seals around thermocouple and power feedthrough ports.

Legacy tests often involved pre-oxidizing cladding segments to emulate surface conditions after operation in reactor by exposing them to 480°C for 30 minutes, which generated a 1-2 µm thick oxide scale on both the interior and exterior surfaces of the cladding. Bare wire type S thermocouples were spot welded to multiple axial and azimuthal locations on the outer diameter of the cladding to monitor temperature gradient effects. For internally heated cladding LOCA tests, the cladding was most often freely suspended into a chamber for testing. The cladding assembly was placed within a heated vessel to ~340°C with the internal heater turned off. The internal heater was turned on to signify the onset of the transient test. Testing was performed with or without an external heating shroud, which tracked the temperature of the fuel pin simulator throughout the temperature transient.

The results of extensive legacy testing include NRC acceptance and represent standard metric for cladding performance during transients [12]. The capability for performing such tests was lost over the last 40 years at ORNL. This work provides a summary of capability redevelopment and a comparison of the current internally heated LOCA test to both the legacy internal heating and current externally heated LOCA test methodologies.

2. MATERIALS AND METHODS

2.1 Initial Design to Re-establish Internal Heater LOCA Rupture Testing

A simplified approach of infrared heating was used for the initial design to re-establish internal heater LOCA test capability at ORNL. This heat source was chosen to allow for much higher heating rates than have been previously reported. Figure 1 shows the computer design of the internal heater test sample next to the finished prototype. The design uses a quartz lamp from the infrared (IR) furnace used for external heating that has been cut and modified to fit inside the test sample. The lamps were specifically ordered to be a reduced size, 8-9mm diameter. As received the lamps were rated for 240V and 1000W encased in clear quartz under vacuum. The lamps had a 10-inch filament heat zone and were 12 inches total. Once received, the lamps were cut down due to the ends and the quartz weld button in the middle of the filament not fitting inside the samples. Once the modifications were done, vacuum was repulled and the lamps were resealed.

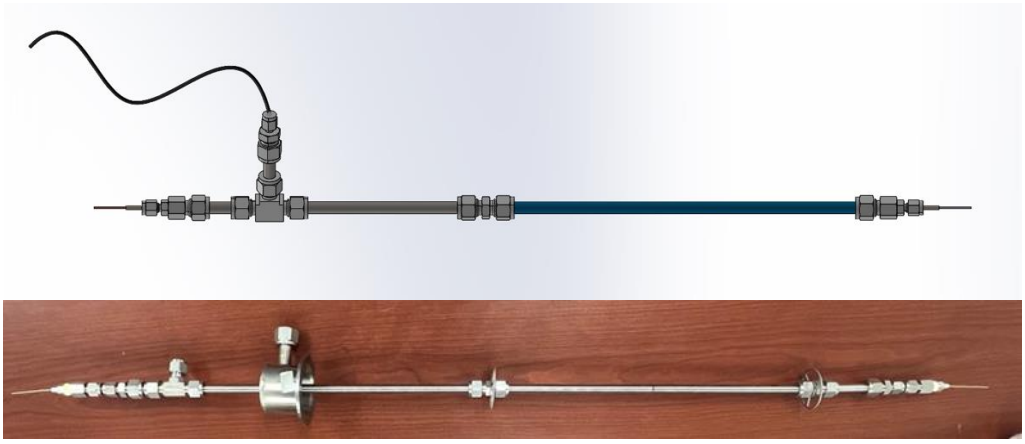

Figure 1. A computer mockup (top) and the first build prototype (bottom) of an internal heater within a 330.2 mm long cladding segment.

The top and bottom of the sample have alumina ceramic insulated National Pipe Taper (NPT) pressure fittings. The fittings allow for power to be conducted through without conducting the sample and leaking pressure. For added protection, a 15A 2 pole breaker was added and the whole assembly was insulation tested to a level of 99.99 MΩ. Heat shrink was used throughout.

2.2 LOCA Burst Testing Comparison between Internal and External Heating Sources

The Severe Accident Test Station (SATS) at ORNL was employed to re-establish the lost capability pursued in this milestone. Conventional SATS LOCA burst tests rely on an external

heat source from a 12-lamp infrared furnace to control the simulated transient. This well-established system was leveraged in this work as a benchmark against the internal heating capabilities. Regardless of heating method, the specimens were subjected to similar experimental conditions, heating rates, and environments.

In this investigation, heating rates of 5°C/s as well as a maximum power output condition were utilized. The cladding segments were filled with an alumina filler rodlet and sealed using Swagelok fittings. A high-pressure connection was established at the top of the cladding, with a transducer maintaining an internal overpressure of ~8.3 MPa. This assembly was freely suspended within the furnace inside a quartz reaction tube. Steam was injected from the bottom of the furnace at room temperature. Specimens were heated to 300°C and maintained at that temperature for five minutes to ensure thermal equilibrium, followed by a temperature ramp until rupture occurred. Temperature was monitored using Type S thermocouples attached to the cladding surface. The control thermocouples was positioned 25 mm above the cladding centerline and a limit thermocouple was placed at the same axial location but 180° oriented from the control. Two additional thermocouples were placed 76 mm above and below the cladding centerline at 0°. The thermocouples were affixed to the cladding with platinum wire. After cladding rupture, the power supply was shut off and the specimens were cooled to room temperature. Cooling air was supplied to the system to rapidly bring the sample temperature below 300°C.

After rupture testing, specimen rupture characteristics (i.e. rupture opening size, cladding diameter strain, rupture location, etc.) were analyzed via optical microscopy. Tubes were then sectioned, mounted in resin, and polished for microstructure analysis. White light and polarized light optical images were taken at the center of the rupture opening cross-section. A segment at the rupture opening was taken for electron backscatter diffraction (EBSD) analysis. EBSD was performed to assess grain size variations between internal and external heat sources at the cladding inner diameter (ID), outer diameter (OD), and center of the cladding wall after testing.

2.3 Validation Testing of Internal Heater with Iron Based Alloys

The validation of high heating rate and internal heating capability was conducted using 16 mm outer diameter and 1 mm wall thickness 316 stainless steel pipe segments, each measuring 330.2 mm in length. Temperature measurements were taken without internal pressure and were assessed across three different heating configurations. In Configuration 1, external heating was provided by 12 infrared heating lamps. Configuration 2 utilized a single filament for internal heating, while Configuration 3 employed a combination of both internal and external heating, featuring a total of 12 lamps—one positioned inside the pipe and the remaining 11 outside in the furnace. All configurations were connected and powered from the same power supply, which supplied maximum power output for each setup. A control thermocouple was positioned at the midpoint of the cladding, accompanied by a limit thermocouple located at the same midpoint but oriented 180 degrees from the control. To monitor axial temperature variations, two more thermocouples were placed 50.8 mm above and below the control thermocouple.

Upon validation of heating capability, a 330.2 mm C26M FeCrAl tube with 9.5 mm OD and 0.38 mm wall thickness was used for initial demonstration LOCA testing. The cladding was retrofitted with an internal heater element inside of a 12-lamp infrared heating furnace, see Figure 3. The specimen was heated externally by 11 halogen filled lamps and the 12th lamp was in series inside of the cladding. A control thermocouple was placed at the center of the sample,

and two additional type S thermocouples were placed 50.8 mm above and below the sample centerline to give an understanding of the temperature profile of the tube. Maximum available power was supplied to the combined internal and external heating sources. The cladding was pressurized to 1200 psi with ultrahigh purity argon at room temperature.

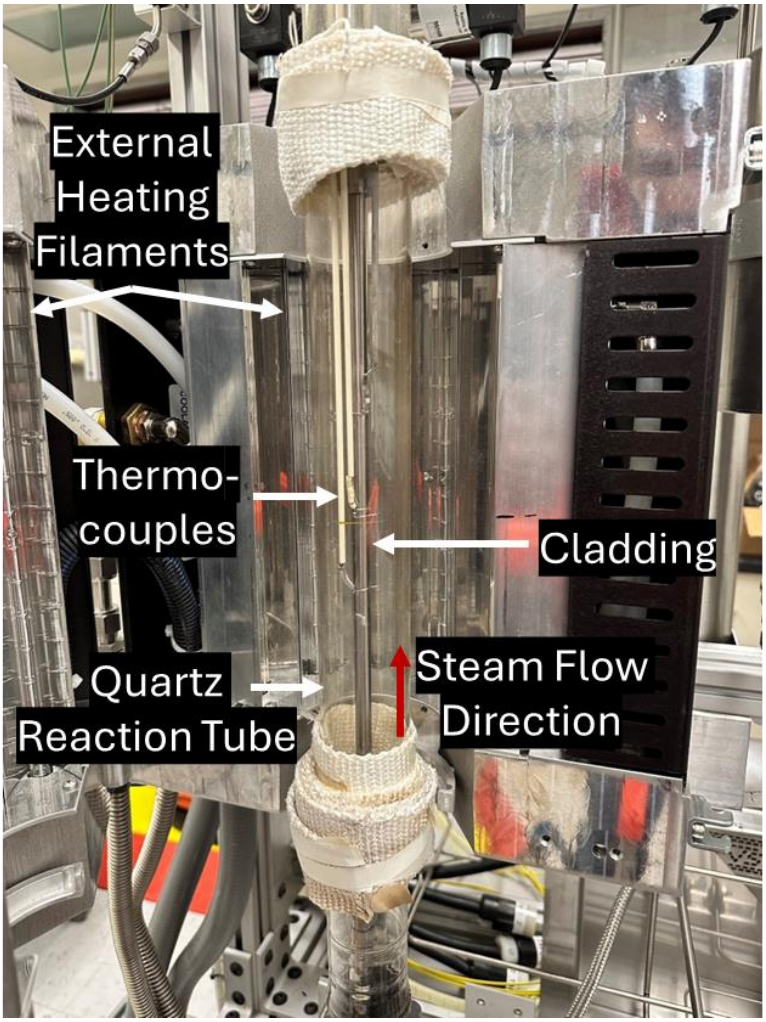

Figure 2. Internal heater specimen inside of the IR furnace.

2.4 Comparative LOCA Testing with Zircaloy-4

For internal-only heating comparison testing, cladding tubes underwent simulated LOCA transients within a stainless-steel vessel to ensure any ejected debris would be contained. Here, 330.2 mm Zircaloy-4 cladding segments were loaded with a heating element and subjected to either 5°C/s or maximum power output conditions. These power conditions were replicated with external-only heating for comparison. All test specimens were heated to 300°C and held for five minutes prior to onset of the temperature transient. Pressure was applied at room temperature and maintained throughout the test until rupture. Externally heating cladding utilized a filler rod, providing ~8% gas volume in the cladding and an infinite gas reservoir to the pressurizing gas

cylinder. Internally heating cladding had ~18% internal gas volume in the cladding and again an infinite gas reservoir from the pressurizing gas cylinder.

3. RESULTS

3.1 Internal Heating Demonstration on 316 Stainless Steel Pipe

316 stainless steel pipe was utilized to investigate the performance of as-purchased filaments. The choice to use stainless steel pipe rather than cladding stemmed from the larger outer diameter of the filaments not allowing insertion into conventional fuel cladding. Future testing with cladding would adapt the filament sheath to fit within a pressurized water reactor (PWR) cladding geometry. Figure 3 illustrates the comparison between external, internal, and combined heating methods across a temperature range of 100°C to 1200°C. Due to the thick-walled nature and greater thermal mass of the stainless-steel tubes, it was anticipated that the resulting heating rates would be slower than those observed with the tested cladding. Temperature profiling with external-only and combined heat sources demonstrated a more rapid initial heat-up at lower temperatures. Conversely, internal-only heating offered a longer duration of high heating rate capability compared to external heating. The average heating rates recorded up to 800°C were 50°C/s for external heating, 82°C/s for internal heating, and 107°C/s for combined heating methods. These findings validated that more prototypic heating rates could potentially be achieved during internally heated fuel cladding LOCA tests and in combined heating tests.

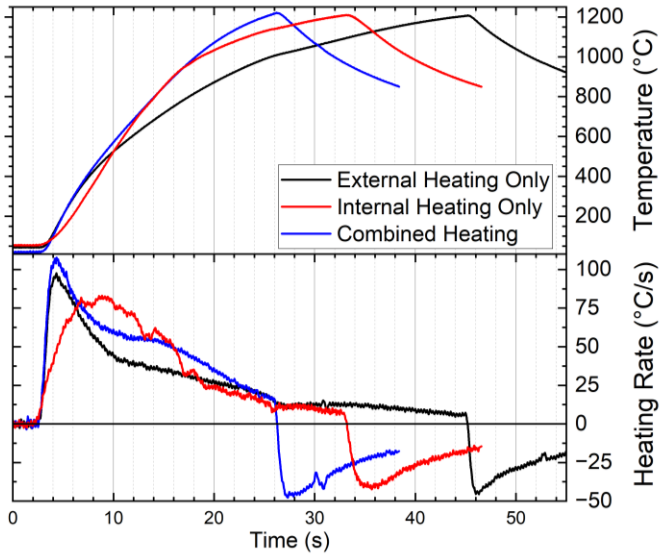

Figure 3. Validation testing of 316 stainless steel pipe without internal pressure, showing both temperature profiles and heating rate profiles.

3.2 Internal and External Heating Initial Demonstration: LOCA Test on C26M FeCrAl Cladding

The first internally heated and internally pressurized test with C26M cladding showed rapid heating of ~150°C/s in the first two seconds, then a slower rate until cladding rupture. The entire test had an average ramp rate of ~100°C/s. Figure 4 shows the rapid heating for the first two seconds then the slower ramp rate for the rest of the test. The center of the cladding was cooler

than the top and bottom. When the element was remanufactured into a smaller glass casing the ends were heated to seal the element and the center was heated to seal the small hole that is used to pull vacuum. The process of remanufacturing the element caused some visible discoloration, related to filament oxidation. The oxidation at the center of the filament may explain why the temperature at the center was not the hottest. Reweld parameters were adapted to mitigate visible discoloration of the filaments for future testing.

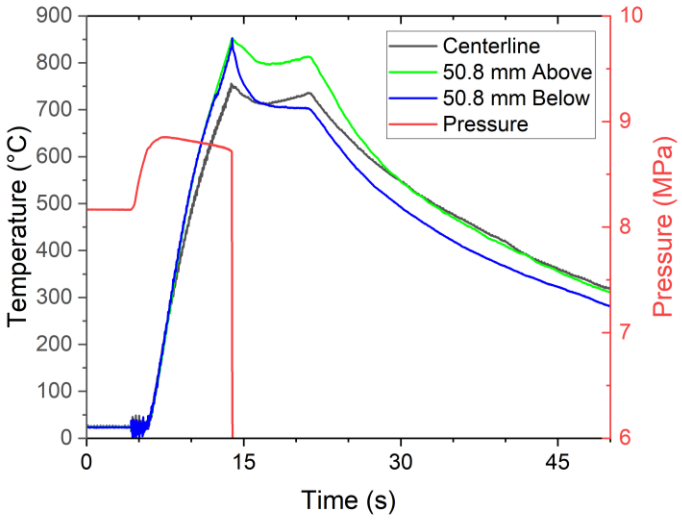

Figure 4. Temperature and pressure profiles for the internal heater demonstration test.

Figure 5 shows the comparison of C26M at 100°C/s in this work to legacy C26M LOCA testing at 5°C/s [13] and 50°C/s [14] with external heating. While changing the ramp rate and internal heating does not dramatically affect the burst temperature, the internally heated cladding datapoint appears to be lower in rupture temperature than the comparable externally heated dataset. Optical photos of the C26M cladding after rupture testing are shown in Figure 6. The tube had localized ballooning with a large burst opening. The rupture and depressurization event caused the tube to bend and shatter the internal lamp. The broken pieces of the lamp put a hole in the back of the tube and broke the reaction tube and the front half of the furnace elements used for the external heating. Due to the oxidized central region of the internal heater, resulting in an uneven temperature distribution, additional characterization was not pursued on the C26M cladding segment.

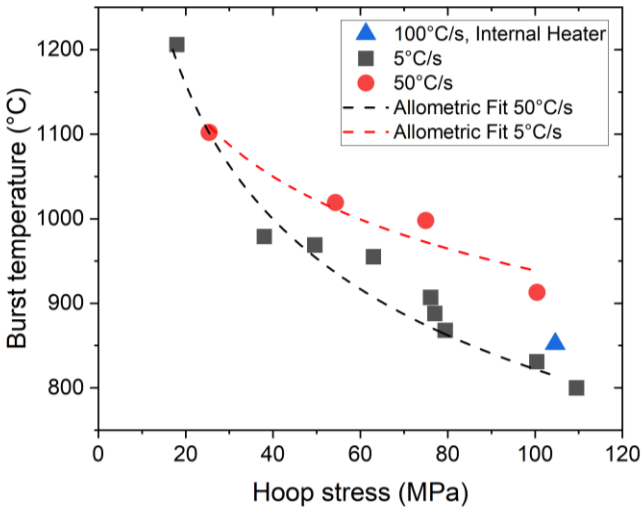

Figure 5. Rupture temperature and rupture pressure for C26M FeCrAl cladding segments.

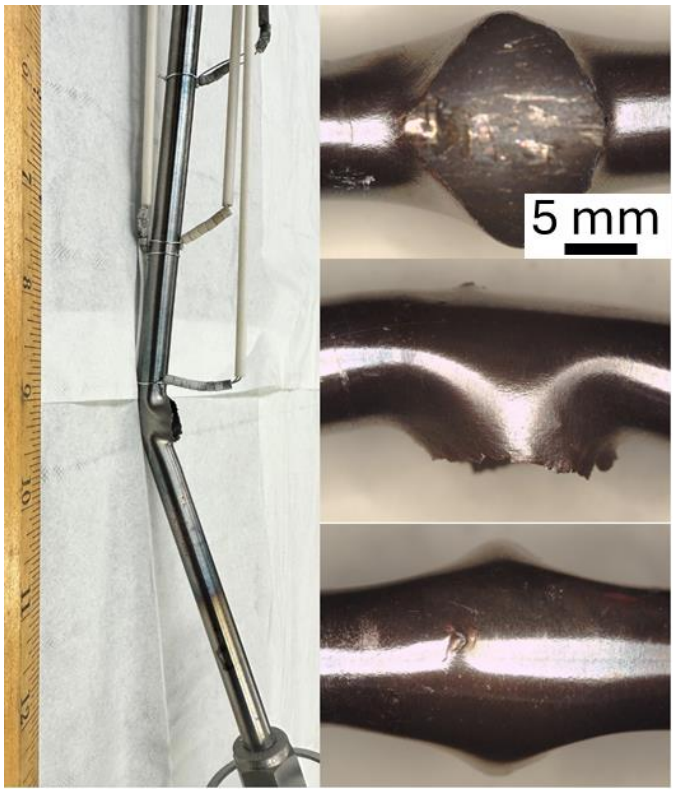

Figure 6. C26M FeCrAl cladding after internally heated LOCA test.

3.3 Internal versus External Heating LOCA Test Comparison

Internal and external heat source LOCA testing were compared for 330.2 mm Zircaloy-4 segments with 5°C/s and a maximum power output, termed a max °C/s heating rate. Temperature and pressure profiles as a function of time are shown in Figure 7 for each test. When comparing the 5°C/s (Figure 7a,b), internal heating resulted in a decreased axial temperature gradient compared to externally heating the cladding. Rupture occurred at similar temperatures. The maximum heating rate externally heating cladding, Figure 7c, showed abnormal discontinuities in the temperature readings within the final seconds prior to rupture. Likely, thermocouple contact was altered during the cladding balloon event. As such, the max °C/s externally heating test was believed to be unreliable in terms of defining an accurate rupture temperature. The maximum power output test with internal heating, Figure 7d, was completed after only a few seconds of testing and incorporated a much higher heating rate than all other tests. Despite the high heating rate, thermocouple readings at the time of rupture were lower than the other tests performed. A summary of test data is presented in Table 1.

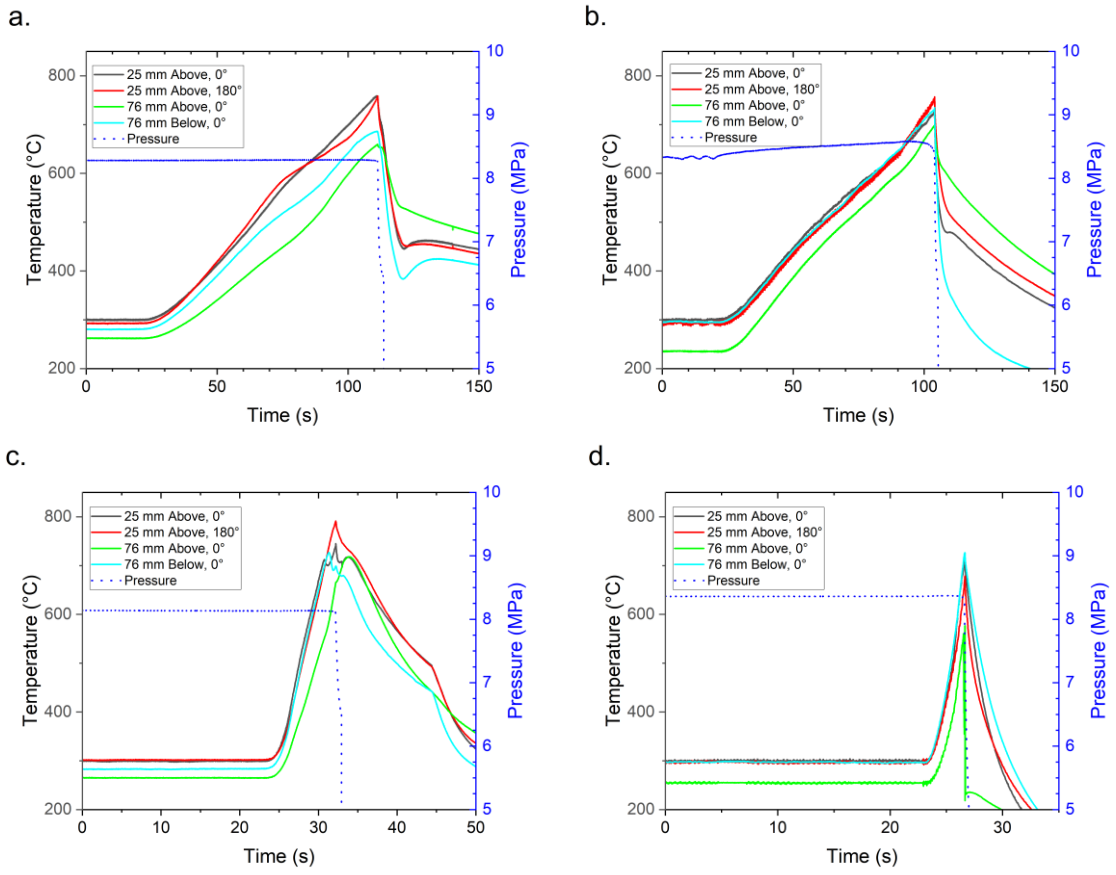

Figure 7. Heating and pressure profiles for a. 5°C/s external heating, b. 5°C/s internal heating, c. maximum °C/s external heating, and d. maximum °C/s internal heating.

Table 1. Cladding rupture properties for internal and external heating tests. *Max °C/s internal heating test showed a nonlinear heating rate.

	5°C/s External	5°C/s Internal	Max °C/s External	Max °C/s Internal
Average Heating Rate (°C/s)	5.7	5.3	69	133*
Average Azimuthal Gradient (°C)	12±8	11±5	28±14	21±21
Average Test Pressure (MPa)	8.3	8.5	8.1	8.4
Maximum Rupture Temperature (°C)	758	757	791	726
Pressure at Rupture (MPa)	8.3	8.2	8.1	7.5

The maximum heating rate internal heater test exhibited a nonlinear heating pattern, with the heating rate increasing throughout the duration of the test. Instantaneous heating and cooling rates, alongside a moving average, are shown in Figure 8. Notably, immediately prior to rupture, the heating rate decreased; however, it remains unclear whether this observation reflects a genuine effect or if it was caused by a change in the contact surface area of the thermocouple bead as the cladding deformed rapidly during a period of plastic instability.

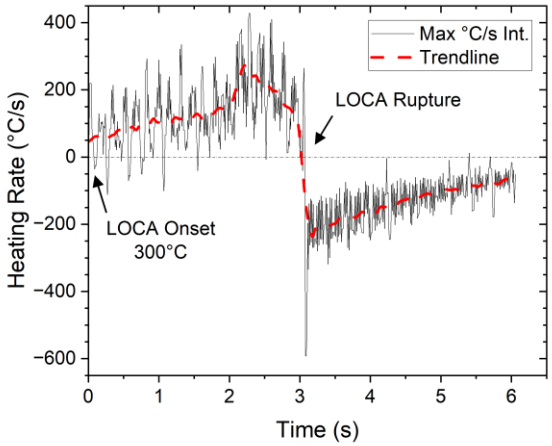

Figure 8. Instantaneous heating rates of Zry-4 cladding during LOCA transient with internal heating and maximum power output.

Figure 9 illustrates the diametric strain profiles of each cladding tube following LOCA testing. The results compare external and internal heating tests across two measurement orientations: 0 and 90 degrees relative to the rupture opening. The 90-degree orientation highlights the deformation in the plane of the rupture event, exhibiting larger magnitudes of total strain. A partial view of the actual specimens after LOCA rupture is also shown in Figure 10. In general, symmetric deformation at the 0 and 90-degree orientations can be seen, with the notable exception of the rupture site itself. Throughout all tests, multiple balloons were observed;

however, the externally heated specimens exhibited additional balloon formations around the thermocouple wire wraps. The internally heated specimens showed multiple balloons along the entire length of the rod. In the maximum heating rate internally heated cladding segment, balloons appeared at regular intervals along the axial length of the cladding, which correlated with the regular spacing of the filament centering rings in the heating element. These centering rings likely generated local hot spots in the cladding. The centering rings appeared to have less effect on the strain results at a heating rate of 5°C/s, likely due to the increased time for heat transfer throughout the cladding segment. Both internally heated specimens exhibited greater degrees of deformation away from the rupture opening site when compared to the externally heated cladding segments.

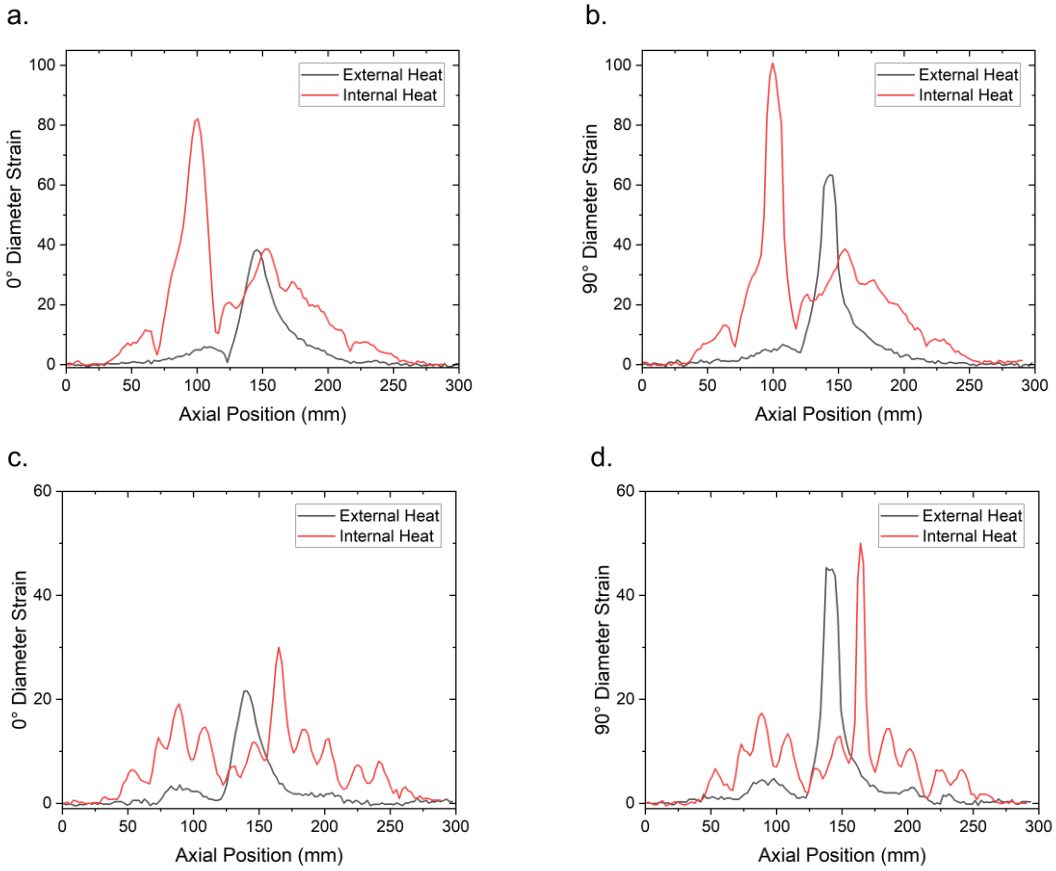

Figure 9. Diameter strain profiles of Zircaloy-4 after LOCA testing, a. 0° orientation diameter strains for 5°C/s internal and external heating, b. 90° orientation diameter strains for 5°C/s internal and external heating, c. 0° orientation diameter strains for max °C/s internal and external heating, d. 90° orientation diameter strains for max °C/s internal and external heating.

Figure 10 illustrates the significant bending of internally heated cladding, a deformation not captured by the diameter strain measurements presented in Figure 9. Rod bending is thought to result from the lack of internal structural support provided by the standard alumina filler rod used in the externally heated cladding tests to counteract temperature gradient effects leading to asymmetric deformation. The rupture openings depicted in Figure 11 further emphasize the distinct differences between the tests conducted with internal and external heating sources. In the external heating tests, the rupture openings exhibit standard geometry consistent with legacy

testing, whereas the internal heating tests reveal a rounded rupture opening geometry. This difference in shape may be attributed to the effects of internal heating, although similar rupture opening shapes have been witnessed with surrogate fuel fragment dispersal testing [15] which suggests the filament ejection upon rupture may govern the opening shape. Rupture-related parameters are tabulated in Table 2.

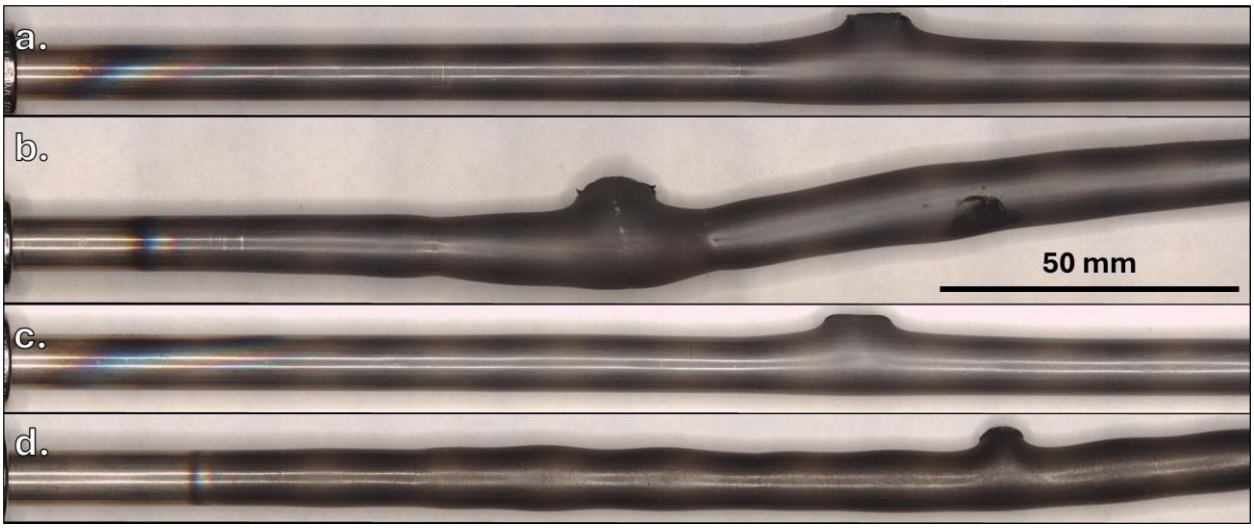

Figure 10. Optical images of the top of the cladding post-LOCA testing, a. 5°C/s externally heated, b. 5°C/s internally heated, c. max °C/s externally heated, and d. max °C/s internally heated.

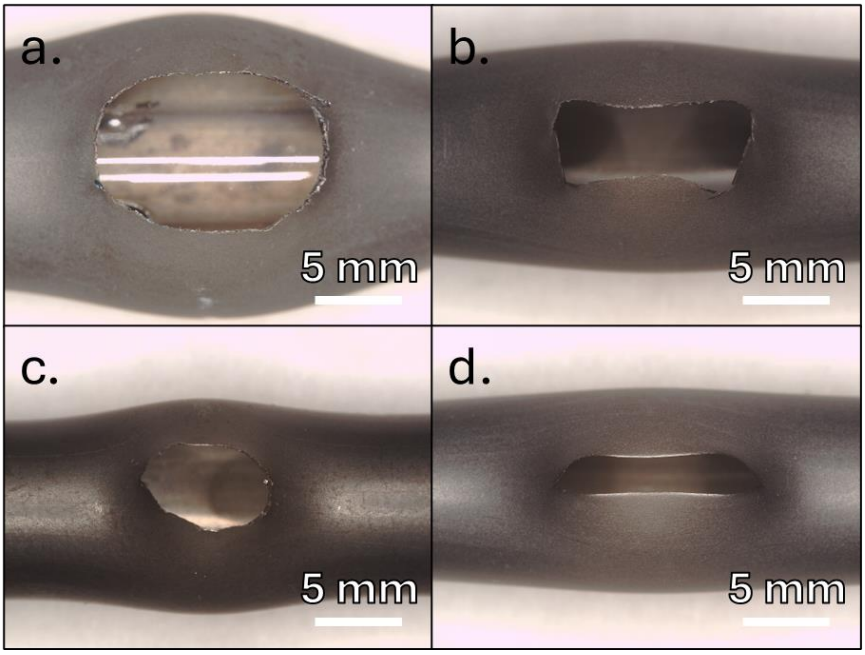

Figure 11. Rupture openings of a. 5°C/s Internal Heating, 5°C/s External Heating, Max °C/s Internal Heating, Max °C/s External Heating.

Table 2. Cladding rupture properties for internal and external heating LOCA testing.

	5°C/s Internal Heating	5°C/s External Heating	Max °C/s Internal Heating	Max °C/s External Heating
Rupture Opening Area (mm^2)	95.7	46.1	26.2	22.2
Rupture Opening Width (mm)	8.91	3.82	4.7	1.94
Rupture Opening Length (mm)	12.91	10.82	7.1	11.51
Maximum Diameter Strain, 0° (%)	82.1	38.4	30.0	21.6
Maximum Diameter Strain, 90° (%)	100.8	63.4	50.1	45.3

Figure 12 and Figure 13 present optical images of the rupture opening cross-sections obtained using both white light and polarized light for internal and external heating tests. The white light images include unique scale bars (as shown in Figures a and b), while all polarized light images at higher magnifications utilize a consistent scale. The internally heated specimens exhibited larger rupture opening widths compared to their externally heated counterparts. Furthermore, the rupture tips of both internally heated segments were bent outward, indicating the cladding depressurization event associated with the rupture, during which the internal heating filament was ejected. Despite these major differences, the grain structure across the cladding segments appeared consistent across all tests.

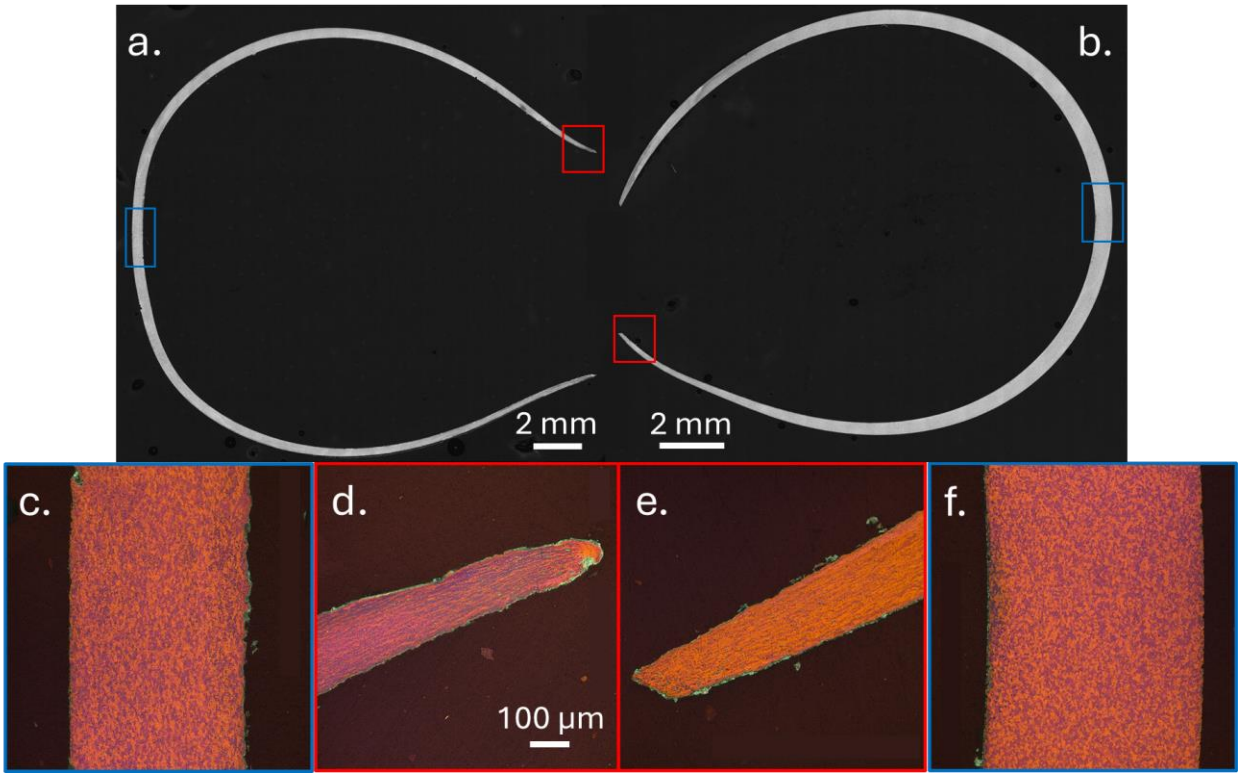

Figure 12. White light and polarized light optical images of the rupture opening cross-section after 5°C/s LOCA testing with (a,c,d) internal heating and (b,e,f) external heating.

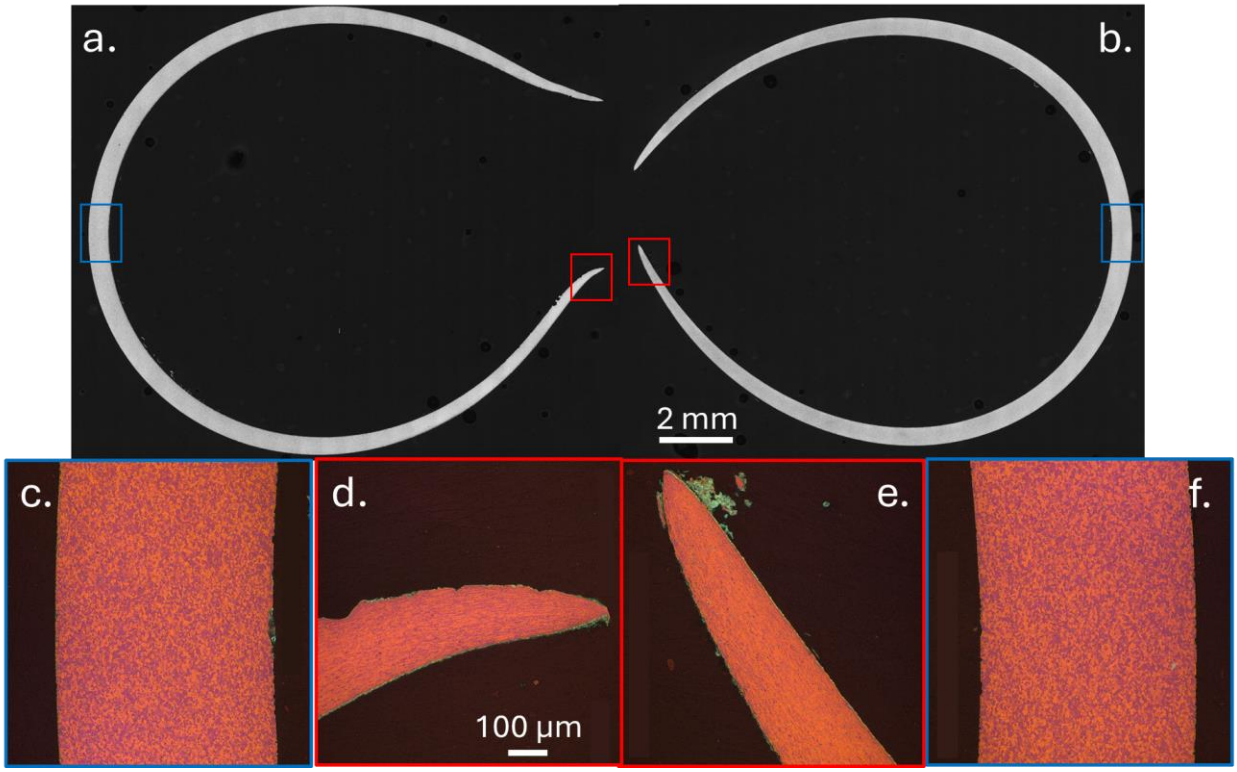

Figure 13. White light and polarized light optical images of the rupture opening cross-section after maximum heating rate LOCA testing with (a,c,d) internal heating and (b,e,f) external heating.

EBSD was performed on all specimens at the ID, OD, and center region of the cladding wall. EBSD inverse pole figures from the center of the cladding are shown in Figure 14. The maps were taken 180° from the rupture opening and the map orientations are perpendicular to the hoop direction. All cladding tubes show similar microstructural features, despite unique heating rates and heat source locations. The average grain sizes for the internal and external heated tests ranged from 3 – 4 µm, with no quantifiable difference between ID, OD, and central wall thickness microstructures. The clear similarities in microstructure clarify that the heat source location does not impact microstructural evolution of the cladding in terms of recrystallization or grain growth.

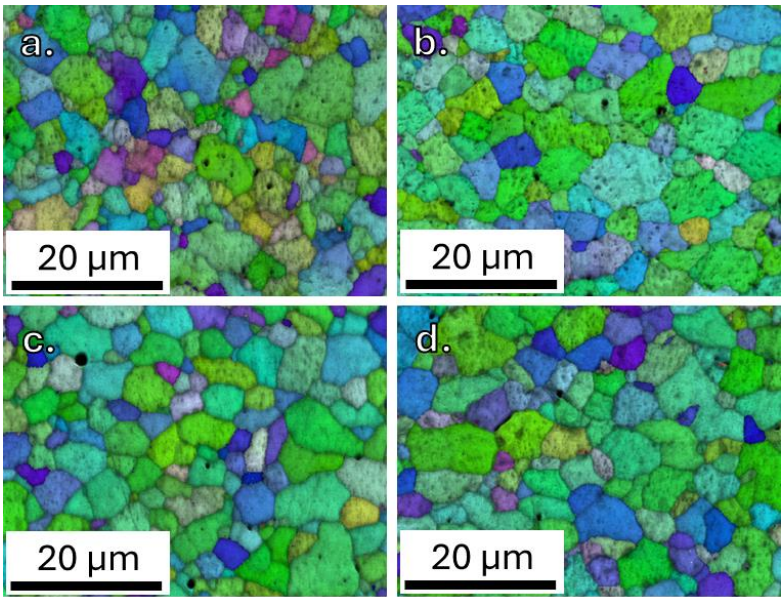

Figure 14. Inverse pole figures from the center of the cladding wall in cross-section, 180° from the rupture opening site. a. internal heating 5°C/s, b. external heating 5°C/s, c. internal heating max °C/s, and d. external heating max °C/s.

The results shown in Figure 9 for the high heating rate specimen deformation were believed to be caused by local temperature increases at internal heater filament centering rings. A simple air heating test was performed on a single Zircaloy-4 rod at 5°C/s and max °C/s heating rates in a new furnace design, in progress, that allowed visualization of the entire cladding segment throughout the transient. Camera images of the cladding tubes during both heating events are shown in Figure 15. It is clear that excess power supplied to the internal heater results in temperature gradients which are producing multiple localized balloons along the axial length of the cladding, as compared to 5°C/s heating rates. As such, future work includes removal of the filament centering rings to improve temperature uniformity with high heating rate LOCA testing.

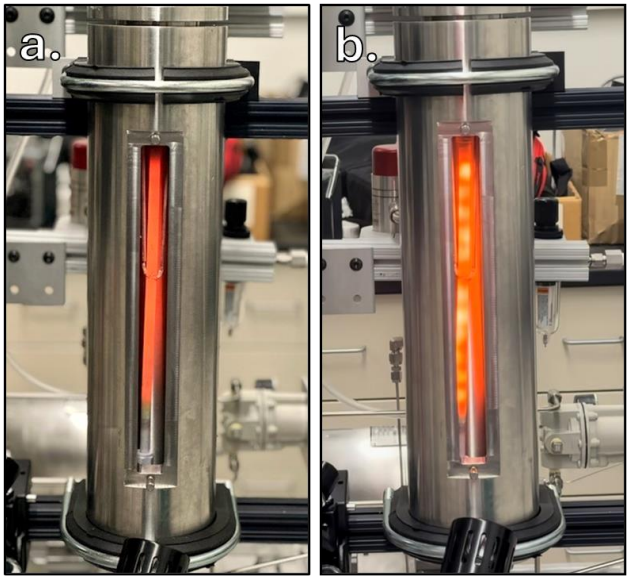

Figure 15. Camera images during a. 5°C/s and b. max °C/s heating in stagnant air.

4. Analysis and Discussion

The present work assesses a simplified and novel design for internal heating of fuel cladding to better represent fuel heating during postulated nuclear accidents. For 5°C/s testing, the rupture temperatures are directly comparable between both heating types, Figure 16. Maximum power output, to receive the highest heating rate possible, showcased unique behaviors compared to the 5°C/s heating tests. Maximum heating tests with the internal heating showed that multiple balloons could form at similar axial locations as the filament centering rings. The filament centering rings appear to serve as localized hot spots every ~20 mm along the cladding length. Due to the very high heating rates utilized for these tests, heat transport throughout the cladding may have been limited. The thermocouple placements relative to the centering rings may not directly reflect the true temperature variation throughout the testing, thus artificially lowering the expected rupture temperature for the maximum °C/s internal heating test. The maximum °C/s external heating test had thermocouple reading errors during the balloon and burst events, which makes such temperature readings inaccurate for this test. Similar testing has been conducted on the same cladding and furnace system, Figure 16, which shows the expected rupture temperature for high heating rate Zircaloy-4 cladding.

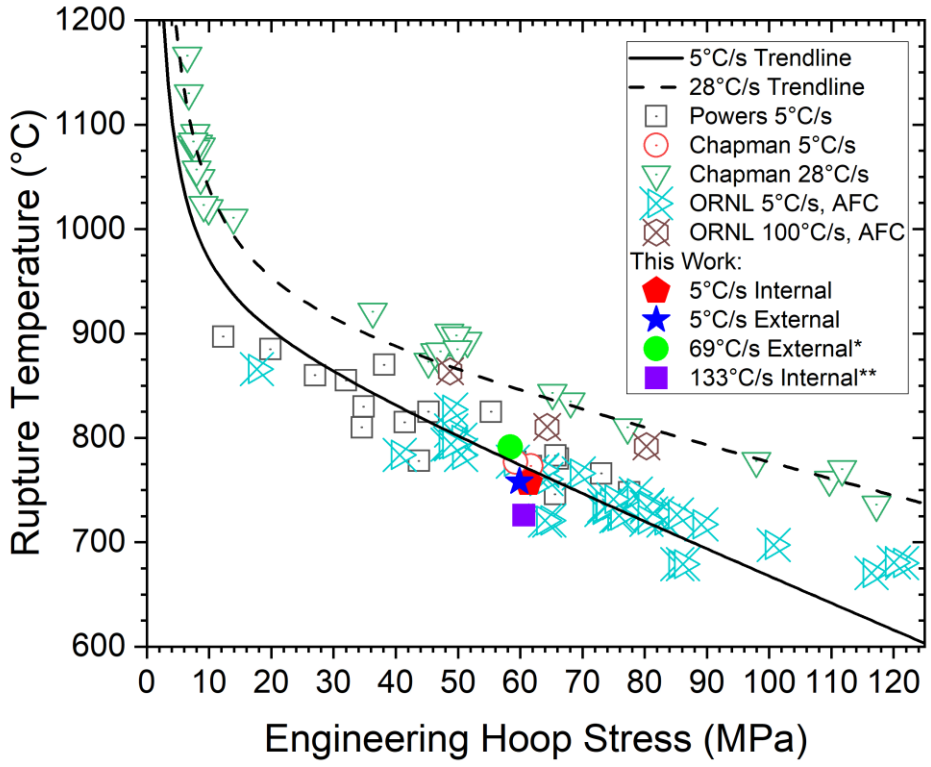

Figure 16. Compilation of rupture temperature and rupture stresses [16,12,17,10,18,19]. *Thermocouple reading abnormalities occurred during the ballooning event, **Cladding outer diameter temperature at thermocouple may not represent maximum temperature of the cladding inner diameter due to the high heating rate.

The balloon sizes observed in the current internal heating tests were larger than those in both the external heating tests and some legacy internal heating studies. When legacy internal heating tests also utilized a heated shroud surrounding a single rod or rod bundle, balloon sizes and circumferential deformation increased to comparable levels as the internal heating test in this work [20], as shown in Table 3. It is therefore likely that the axial and azimuthal temperature profiles, in addition to the heating rate, are primary factors for governing rod deformation character, as has been shown by Erbacher and coworkers [21]. The internal gas volumes of the internally and externally heated tubes in this work were similar, suggesting that temperature uniformity in addition to filament ejection during rupture likely contribute more to the observed differences in balloon formation.

Table 3. Comparative summary of cladding rupture diameter strains with similar legacy test data using internal heating [11,12,22,23].

	Heating Rate (°C/s)	Rupture Temperature (°C)	Rupture Pressure (MPa)	Maximum Diameter Strain (%)	Notes
Internal Heating	5	757	8.2	100.8	This work
External Heating	5	758	8.3	63.4	This work
SR-43	4	773	7.6	29	Out of pile, single rod, steam atmosphere
SR-44	5	777	7.3	30	
SR-49	5	783	7.6	95	Out of pile, single rod, heated shroud, steam atmosphere
SR-64	5	766	8.5	110	
SR-65	5	748	9.0	74	
Internal Heating	133	726	7.5	50.1	This work, low OD temperature reading
External Heating	69	791	8.1	45.3	This work, thermocouple reading issues during balloon/burst
SR-5	28	810	9.5	26	Out of pile, single rod, steam atmosphere
SR-28	28	835	8.4	27	
SR-29	28	843	8.1	27	
B-1-1	29	852	7.8	36	Out-of-pile, 16-rod bundle, heated shroud, steam atmosphere.
D-2-15	29	836	7.9	35	Out-of-pile, 16-rod bundle, steam atmosphere.

For comparison, one legacy internal heating test conducted by Chapman and colleagues [11] was digitized and overlaid with the current 5°C/s internal heating test, as shown in Figure 17. Both tests were internally pressurized to approximately 8 MPa and utilized a 5°C/s heating rate until cladding rupture occurred, at which point the heating power was turned off, and the system was allowed to cool back to room temperature. A minor pressure difference between the two tests resulted in a slight shift in rupture temperature, although the difference is deemed negligible when comparing rupture temperature and engineering hoop stress of these tests on Figure 16. To compare the azimuthal temperature gradient throughout the LOCA testing, both tests included thermocouples positioned at 0° and 180°. Figure 17b illustrates the azimuthal temperature gradient as a function of test time, demonstrating that the gradient remained comparable throughout the entire test until the rupture point.

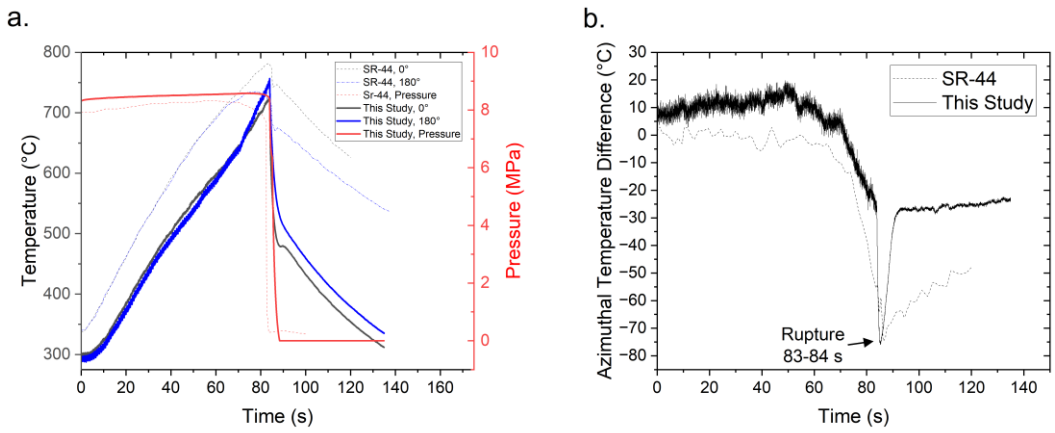

Figure 17. Comparison of internally heated Zircaloy-4 rods at 5°C/s heating rates from this study and from literature, digitized by the authors from [11].

The current internal heating capability successfully demonstrated the ability to reproduce rupture temperatures for 5°C/s heating rate LOCA experiments. Notable differences from legacy data, such as balloon geometry and rupture opening geometry, will be thoroughly addressed to ensure that all relevant test parameters are well understood and adequately captured in future experiments. Below is a list of ongoing upgrades for further investigation.

Currently, the internal heating filaments are encased in quartz under vacuum. To prevent filament ejection, the quartz casing will be replaced with a high-temperature metal casing. This upgrade is expected to restore the anticipated rupture opening geometry by eliminating particulate ejection. Additionally, the added structural support from the metal casing will help mitigate tube bending during the rupture event. The casing diameter could be modified to provide control of the internal gas volume as an additional modifying parameter during LOCA testing.

The filament centering rings have produced localized temperature variations along the axial length of the cladding, resulting in multiple balloons forming along the internally heated cladding segments. Therefore, future work will involve removing all centering rings. To enhance the understanding of cladding rupture under high heating rates, the SATS furnace used for internal heating tests will be equipped with a viewport for digital image correlation.

While other SATS furnaces have demonstrated significant benefits from in situ deformation analysis via digital image correlation (DIC) [17,10,19,24], the current viewport was limited to approximately 38 mm to minimize heat loss from the external heating elements. Future enhancements to the internal heating capability will allow for almost a full view of the 330.2 mm cladding segment during transient LOCA or creep testing, as shown previously in Figure 15. Additionally, pressure control systems are being upgraded to enable a broader internal pressurization range of up to 6,000 psi, which will expand the research and development scope for material property assessments using DIC data.

The present work evaluated a controlled heating rate of 5°C/s and a less controlled maximum power output to establish bounding cases for future testing. Future investigations will focus on thermal gradient effects at intermediate heating rates (i.e., 5 – 100°C/s), as more data is available for direct comparison within this range.

5. SUMMARY

After around 40 years of lost capability, internally heated fuel cladding transient test capability has been re-established at ORNL, utilizing a simplified design that offers a cost-effective and high-throughput approach for conducting internally heated LOCA tests. Current results indicate that rupture temperatures from internal and external heating LOCA tests are comparable and consistent with legacy data. Additionally, the heating profiles and rupture temperatures align between current and legacy tests conducted at a rate of 5 °C/s using internal heating. However, the present internal heating methodology, which employs a quartz-sheathed filament, led to particulate ejection during rupture. This phenomenon is believed to increase the size and shape of the rupture opening compared to traditional trends. Additionally, heating rates exceeding 100 °C/s caused multiple cladding balloons due to local temperature fluctuations generated by the filament centering rings within the internal heater. It is hypothesized that the cladding cannot distribute heat rapidly enough at such high rates, resulting in multiple small balloon regions and an artificially low rupture temperature. Ongoing efforts will involve replacing the quartz sheath to reduce particulate ejection and modifying the filament winding to better control local temperature uniformity along the axial length of the rodlets. Further, thermocouple placement within the cladding during internal heating tests will provide clarity on heat transport through the cladding wall to determine if heat transport is a limiting factor when conducting transient tests above 100°C/s.

6. ACKNOWLEDGEMENTS

The authors gratefully acknowledge the help of E. Powers and D. Wilson for electrical work related to internal heating capability development, J. Horenburg for specimen metallographic preparation, T. Lowe for characterization, and Y. Yan and J. Han for internal review. This work was supported by the U.S. Department of Energy, Office of Nuclear Energy.

7. REFERENCES

[1] C. Lemaignan, 2.07 - Zirconium Alloys: Properties and Characteristics, in: R.J.M. Konings (Ed.), Compr. Nucl. Mater., Elsevier, Oxford, 2012: pp. 217–232. https://doi.org/10.1016/B978-0-08-056033-5.00015-X.

[2] B.A. Pint, K.A. Terrani, M.P. Brady, T. Cheng, J.R. Keiser, High temperature oxidation of fuel cladding candidate materials in steam–hydrogen environments, J. Nucl. Mater. 440 (2013) 420–427. https://doi.org/10.1016/j.jnucmat.2013.05.047.

[3] H.M. Chung, T.F. Kassner, Deformation Characteristics of Zircaloy Cladding in Vacuum and Steam under Transient-Heating Conditions: Summary Report, Argonne National Laboratory, 1978.

[4] R.H. Chapman, Multirod burst test program quarterly progress report for April--June 1976. [BWR; PWR], Oak Ridge National Lab., Tenn. (USA), 1977. https://www.osti.gov/biblio/7232563 (accessed May 8, 2025).

[5] D.A. Powers, R.O. Meyer, Cladding swelling and rupture models for LOCA analysis, (1979).

[6] R.A. Lorenz, D.O. Hobson, G.W. Parker, FUEL ROD FAILURE UNDER LOSS-OF-COOLANT CONDITIONS IN TREAT., Nucl Technol 11 No 4 502-20Aug 1971 (1971). https://www.osti.gov/biblio/4843984 (accessed May 8, 2025).

[7] R.A. Lorsnz, W. Parker, Final Report on the Second Fuel Rod Failure Transient Test of a Zircaloy-Clad Fuel Rod Cluster in TREAT, (1972). https://doi.org/10.2172/4691610.

[8] D.-H. Kim, G.-H. Choi, H. Kim, C. Lee, S.-U. Lee, J.-D. Hong, H.-S. Kim, Measurement of Zircaloy-4 cladding tube deformation using a three-dimensional digital image correlation system

with internal transient heating and pressurization, Nucl. Eng. Des. 363 (2020) 110662. https://doi.org/10.1016/j.nucengdes.2020.110662.
[9] Z. Duan, B. Yuan, Q. Wen, R. Zhang, K. Chen, Effects of internal pressure and heating rate on the burst behaviors of Cr-coated cladding during simulated LOCA testing, Ann. Nucl. Energy 204 (2024) 110548. https://doi.org/10.1016/j.anucene.2024.110548.
[10] M. Ridley, C. Massey, S. Bell, N. Capps, High temperature creep model development using in-situ 3-D DIC techniques during a simulated LOCA transient, Ann. Nucl. Energy 193 (2023) 110012. https://doi.org/10.1016/j.anucene.2023.110012.
[11] R. Chapman, J. Crowley, A. Longest, E. Sewell, Effect of creep time and heating rate on deformation of Zircaloy-4 tubes tested in steam with internal heaters, 1978. https://doi.org/10.2172/6555543.
[12] D.A. Powers, R.O. Meyer, Cladding swelling and rupture models for LOCA analysis Technical report, Nuclear Regulatory Commission, United States, 1980.
[13] S.B. Bell, K.A. Kane, C.P. Massey, L.A. Baldesberger, D. Lutz, B.A. Pint, Strength and rupture geometry of un-irradiated C26M FeCrAl under LOCA burst testing conditions, J. Nucl. Mater. 557 (2021) 153242. https://doi.org/10.1016/j.jnucmat.2021.153242.
[14] S.B. Bell, M.J. Ridley, N.A. Capps, R.T. Sweet, Y. Yamamoto, C.P. Massey, Recrystallization Driven Softening and Heating Rate Dependencies of FeCrAl Nuclear Fuel Cladding during Accident Transients, Materialia (2025) 102432. https://doi.org/10.1016/j.mtla.2025.102432.
[15] Mackenzie Ridley, P.J. Doyle, N. Capps, Out-of-Cell Fuel Dispersal Characterization, Oak Ridge National Laboratory, Oak Ridge, TN (United States), 2023.
[16] R.H. Chapman, Multirod Burst Test Program quarterly progress report, April--June 1977. [BWR; PWR], Oak Ridge National Lab., Tenn. (USA), 1977. https://www.osti.gov/biblio/5287241 (accessed May 22, 2025).
[17] K. Kane, S. Bell, B. Garrison, M. Ridley, M. Gussev, K. Linton, N. Capps, Quantifying deformation during Zry-4 burst testing: a comparison of BISON and a combined in-situ digital image correlation and infrared thermography method, J. Nucl. Mater. 572 (2022) 154063. https://doi.org/10.1016/j.jnucmat.2022.154063.
[18] S. Bell, Toward Accelerated Qualification of ATF Claddings: An In-Situ Burst Testing Framework and Insights into Zr Alloy LOCA Behavior, Dr. Diss. (2023). https://trace.tennessee.edu/utk_graddiss/9050.
[19] S.B. Bell, K.A. Kane, M.J. Ridley, B.E. Garrison, B.S. Johnston, N.A. Capps, *In-situ* determination of strain during transient burst testing and the temperature dependence of Zircaloy-4 claddings, J. Nucl. Mater. 591 (2024) 154910. https://doi.org/10.1016/j.jnucmat.2024.154910.
[20] A.W. Longest, Multirod Burst Test Program Progress Report for January - March 1979, Oak Ridge National Laboratory, 1979. https://www.nrc.gov/docs/ML1920/ML19209B062.pdf.
[21] F.J. Erbacher, S. Leistikow, Zircaloy fuel cladding behavior in a loss-of-coolant accident: a review, Zircon. Nucl. Ind. (1987). https://asmedigitalcollection.asme.org/astm-ebooks/book/chapter-pdf/7183001/10_1520_stp28138s.pdf (accessed May 15, 2025).
[22] R.H. Chapman, Multirod Burst Test Program progress report, July--December 1977. [BWR; PWR], Oak Ridge National Lab., Tenn. (USA), 1978. https://www.osti.gov/biblio/6767244 (accessed January 26, 2022).
[23] R.H. Chapman, D.O. Hobson, J.L. Crowley, A.W. Longest, Multirod Burst Test Program BUNDLE B-1 TEST DATA Interim Report, ORNL/NUREG/TM-322 (1979).
[24] S.B. Bell, M.J. Ridley, C.P. Massey, N.A. Capps, Step-loaded creep testing of Zircaloy-4 cladding at higher temperatures in the α-phase, Acta Mater. (2025) 120821. https://doi.org/10.1016/j.actamat.2025.120821.